J. Physiol. (1980), **309**, *pp.* 499–519
With 11 *text-figures*
Printed in Great Britain

ASYMMETRY CURRENTS IN THE MAMMALIAN MYELINATED NERVE

BY S. Y. CHIU

From the Department of Pharmacology, Yale University School of Medicine, New Haven, Connecticut 06510, U.S.A.

(*Received 21 December 1979*)

SUMMARY

1. Asymmetrical displacement currents were recorded in the rabbit node of Ranvier by averaging the currents associated with depolarizing and hyperpolarizing pulses in the temperature range 15–25 °C with the ends of the fibre cut in 160 mM-CsCl.

2. The identification of the asymmetrical currents as intramembranous current is supported by the findings that (*a*) the 'on' and 'off' current transients were equal for short and small depolarizing pulses and (*b*) the total charge displaced reached saturation at (32–111 $\times 10^{-15}$ C/node) when sufficiently large depolarizations were applied.

3. After a large depolarization to around 50 mV, the 'off' response consisted of a fast phase followed by a slow phase. Lengthening the depolarization reduced the size of the fast response but enhanced the slow response.

4. The steady-state rearrangement of the charges can be described by a Boltzmann distribution of charges with an effective valence of 1·86 and a midpoint potential of − 33 mV. The time course of rearrangement of these charges following a change in membrane potential could be fitted reasonably well with a single exponential though a double exponential might have been better at large depolarizations.

5. The steady-state activation curve for Na conductance was measured with various procedures to eliminate the effects of series resistance, which include decreasing peak Na current by TTX, and electronic compensation of the series resistance. The measured steepness of the Na-activation curve corresponds to moving a minimum charge of about $5\bar{e}$ to open each Na channel at 22·7 °C.

6. The time constant (τ_m) for activation of Na current and time constant (τ_{on}) for declining phase of the asymmetry current were of the same order of magnitude but not identical over the potential range − 50 to + 25 mV.

7. The time course of charge displacement determined from the asymmetry current occurred earlier than did Na activation. Raising the charge displacement curve to second or third power did not yield a curve that matched the time course of Na activation.

8. If all the observed asymmetrical currents are related to the Na-gating system, an upper limit for the number of Na channels per rabbit node is 82,000 and a lower limit for the single channel conductance is 9·8 pS at 18·8 °C.

0022-3751/80/2940-0691 $07.50

INTRODUCTION

Armstrong & Bezanilla (1974) and Keynes & Rojas (1974) first measured a small asymmetrical current in the squid axon resulting from displacement of charged particles within the nerve membrane that is believed to reflect the activation mechanism of Na channels (see also Meves, 1974; Nonner, Rojas & Stämpfli, 1975; Cahalan & Almers, 1979). Subsequently, such asymmetrical currents have been found in frog myelinated nerve (Nonner *et al.* 1975), in *Myxicola* giant axons (Rudy, 1976), in *Aplysia* (Adams & Gage, 1976) and in *Helix* neurones (Kostyuk, Krishtal & Pidoplichko, 1977).

This paper reports measurement of such asymmetry currents in single mammalian nodes of Ranvier. This measurement is of particular interest, since in most mammalian myelinated nerves the K currents are very low or absent (Horackova, Nonner & Stämpfli, 1968; Chiu, Ritchie, Rogart & Stagg, 1979*b*; Brismar, 1979; Chiu & Ritchie, 1980) and this raises the question of whether the kinetics of the mammalian asymmetry currents are any different than in frog and squid nerve. In the present investigation, no significant differences were in fact found. On the assumption that all the observed asymmetry currents reflect activation of mammalian Na channels, it is concluded that (*a*) the asymmetry charge movement cannot be the physical correlate of the '*m*' parameter of the Hodgkin-Huxley equations, (*b*) there are, at most, 40,000–139,000 channels in a rabbit node (of about 20 μm diameter), the conductance of each of which being at least 9·6 pS at 15–23·4 °C.

METHODS

Voltage clamp studies were conducted at 15–25 °C by the method of Dodge & Frankenhaeuser (1958) as modified by Hille (1971). The potentiometer amplifier is of a modified design, and a shield was used over the A–B partitions (see Sigworth, 1980). Large single myelinated fibres (diameters 18–22 μm) from rabbit sciatic nerves were dissected and mounted as described previously (Chiu *et al.* 1979*b*). The temperature in the immediate vicinity of the node was measured continuously by a fine thermocouple (50 μm diameter) which was implanted permanently in the Perspex nerve chamber and which lay 1 mm directly below the node. Temperature control was achieved by circulating liquid at a fixed temperature through the brass block enclosing the nerve chamber. All preparations were allowed to stablize in the brass block for 10–15 min before kinetic measurements were begun. The holding potential was then adjusted to give a resting inactivation of about 0·25 (h_∞ = 0·75), and the corresponding absolute membrane potential is assumed to be −80 mV (Chiu *et al.* 1979*b*).

Solutions. The solution bathing the rabbit node was composed of (mM): NaCl, 154; $CaCl_2$, 2·2; KCl, 5·6; and MOPS buffer (pH 7·4), 10. Na-free solutions were prepared by replacing all the external NaCl by an equiosmotic amount of either TEA-Cl or TMA-Cl plus 300 nM-TTX to block the sodium channel. The ends of the fibres in most experiments (C and E pools; for example, see Fig. 1. Chiu *et al.* 1979*b*) were cut in 160 mM-CsCl. For reasons still unclear to us, cutting a mammalian fibre in CsCl rather than KCl seemed to enhance the survival rate of these fibres.

Experimental protocol. The aim of this paper was to measure asymmetry current in rabbit nodes of Ranvier, and to obtain limiting values for the number of sodium channels and the single channel conductance in a rabbit node by measuring the total Na gating charge movement (Q_{max}) and the maximum Na conductance ($\bar{G}_{Na}$) in the same fibre. The Na and asymmetry currents were calibrated by measuring the internodal resistances after each experiment as described previously (Chiu *et al.* 1979*b*). The command pulse sequence and the storage of the current responses in the computer were controlled by a PDP11/70 computer. A programmable

stimulator (PSG-1, Page Digital Electronics) provided both the pulse sequence to the voltage clamp and the sample commands to the analogue-to-digital converter.

Measurements of $\bar{g}_{Na}$ and instantaneous I–E relations. At the beginning of each experiment, the relation between peak Na current and voltage was determined from a series of depolarizations preceded by a hyperpolarizing prepulse to −125 mV with series resistance compensation (see

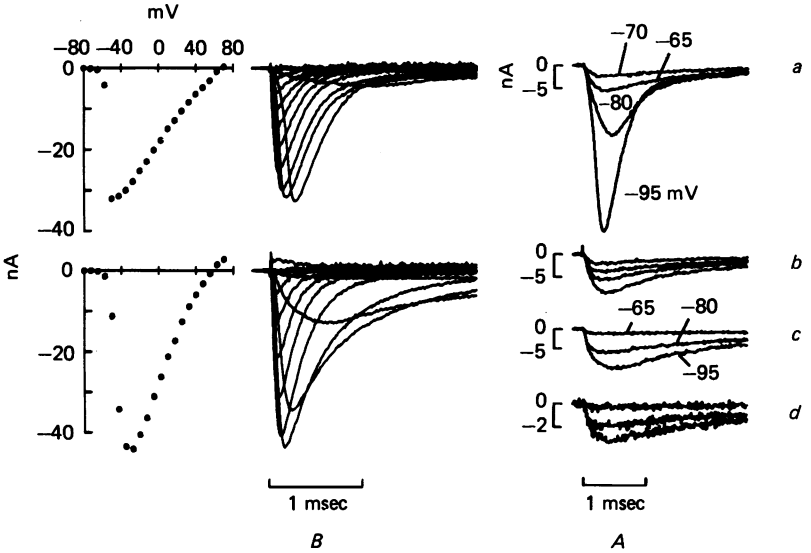

Fig. 1. Effect of series resistance compensation on Na current. The ends of the fibres were cut in 160 mM-CsCl. Temperature 25 °C. *A*, in each of the four panels are superimposed Na current records associated with a fixed depolarization to −50 mV preceded by various prepulses as indicated. The test depolarization to −50 mV is around the steepest part of the negative-slope region of the current–voltage relation for peak Na current and the current should be most sensitive to series resistance error. This can be seen in panel (*a*): changing the current sizes with different prepulses resulted in currents with different shapes. In panel (*b*) resistance compensation was adjusted (corresponding to 0·7 MΩ) until all currents had similar shapes irrespective of sizes. In a different experiment, the compensated currents (*c*) were compared with that obtained after resistance compensation was removed and a small amount of TTX was added to block 70 % of the current (*d*). Two points are noted. First, in contrast to (*a*), various prepulses now yielded currents of similar shapes after depression of currents by TTX (*d*). Secondly, since the compensated currents (*c*) are similar in shape to that of the TTX-treated current (*d*), the criterion used in adjusting the compensation (*b*) is justified. *B*, the two panels show two families of Na current from a different fibre with (lower) and without (upper) series resistance compensation. The series of depolarizations used were preceded by a 40 msec hyperpolarizing prepulse to −110 mV. The corresponding depolarization for each current trace can be noted from *C*, which shows the corresponding current–voltage relations.

below). From this measurement the hypothetical limiting value of $\bar{g}_{Na}$ was determined using the Na current associated with a depolarization to −5 mV, after correcting for Na inactivation and assuming that activation was maximal as described previously (see p. 157 of Chiu *et al.* 1979*b*). Inactivation of the Na current was fitted to the function $y = A \exp(-\alpha t) + C$ by least squares, in a FORTRAN program employing linearization of parameters. The instantaneous *I–E* measurements employed a 0·2–0·5 msec activating pulse to around +50 mV chosen to be near E_{Na} (Table 2) in order to activate Na conductance with a minimum of ion-accumulation effects. The sampling interval for the current monitor signal was 10–50 μsec in the peak *I–E* measurement and was 6 μsec in the instantaneous *I–E* measurement.

Series resistance compensation. The method of Sigworth (1980) for compensating nodal series resistance was used here. The criterion for setting the series resistance compensation was that the compensated sodium current at the mid-point potential of the activation curve for sodium conductance (about −50 mV) had about the same shape when the size of the current was changed by about 80%, hyperpolarizing prepulses to between −80 and −125 mV and depolarizing prepulses to −65 mV being used. Fig. 1*A*, *a* shows superimposed Na current records at −50 mV (before compensation) when various prepulses were used to change the size of the currents. The shape of the larger currents (hyperpolarizing prepulses) are obviously distorted by series resistance. Fig. 1*A*, *b* shows the result of adjusting the series resistance compensation until the larger currents are 'under control', i.e. have similar shape as the smaller currents. This criterion of adjusting series resistance compensation was justified by Fig. 1*A*, *c* and *d* (from a different experiment) which shows that blocking about 70% of the current by TTX (thus reducing series resistance error by 70%) in the absence of series resistance compensation did indeed yield sodium currents of similar shape by prepulses (Fig. 1*A*, *d*). Furthermore, the TTX-treated Na currents had almost identical shape as the compensated Na currents (Fig. 1*A*, *c*). Fig. 1*B* shows two families of Na current before (upper) and after (lower) series resistance compensation. *C* shows the corresponding *I–E* relation for the Na currents.

Uncertainty in series resistance compensation. The average value for the series resistance used n the compensation is 0·76 MΩ in this paper. The setting for the series resistance in individual experiments (for example, as is done in Fig. 1*A*, *b*) was somewhat arbitrary, and, typically, changing the setting by about ±0·12 MΩ around the chosen setting usually did not lead to any significant changes in the shapes of the currents. This change of ±0·12 MΩ in the setting would result in a change of ±3·6 mV around −5 mV, calculated using the average peak Na current of 30 nA at this potential (Table 2) and ignoring a much smaller leakage. With E_{Na} = 61 mV (Table 2), the corresponding change in size of the compensated current at −5 mV would be about ±5% (i.e. ±3·6/66).

The present method of compensating for the series resistance assumes first, that the distortion of the larger current in Fig. 1*A*, *a* is the result of an external series resistance in series with an homogeneous population of Na channels, and, secondly, activation and inactivation kinetics are independent (i.e. different prepulses should yield Na currents of similar shapes at a fixed depolarization). In the worst case when these two assumptions fail, calculation of $\bar{g}_{Na}$ using the uncompensated current, which would yield values about 30% smaller than that in Table 2, may have been better (for example, compare compensated and uncompensated current at −5 mV in Fig. 1*C*).

Measurement of gating current. A conventional technique (e.g. Nonner *et al.* 1975) of averaging nodal currents with pulses of different polarity was used to measure the asymmetry currents. Both the positive and negative pulses were applied from the same reference potential (between −102·5 and −110 mV) that was more negative than the resting potential, and the nodal membrane was held at this potential between the subsequent gating current records; the frequency of stimulation was usually less than 4 sec^{-1}. Positive and negative pulses of similar size were used if the positive step did not exceed −20 mV. With larger positive pulses, smaller negative pulses to −(140–170) mV were used. The current signal was sampled every 5–8 μsec and 40 samples were taken before the test pulse for the baseline. Typically, the currents in response to ten individual positive pulses and 10–30 negative pulses were averaged. The associated asymmetry current was calculated on line by adding to the positive current response an appropriately scaled negative response, and displayed on the computer screen for inspection. The procedure was then repeated and a cumulative average obtained. Usually the noise level of the cumulative average of the asymmetry current record was deemed satisfactory after three groups of positive and negative pulses (i.e., 30 positive and 30–90 negative steps). Unless otherwise mentioned the current monitor signal was filtered by a 33 kHz 4-pole Bessel filter in series either with a RC filter of time constant 8 μsec or with a 2-pole Bessel filter with a cut-off frequency of 33–22 kHz,

Analysis of asymmetry current records. A typical 'on' asymmetry current record (for example, see Fig. 3*A*) showed a more-or-less monotonic declining phase which was preceded by an initial rise that reached its peak within 20–30 μsec. This rising phase is most likely due to the finite settling time of the voltage-clamp and the low-pass filter (for example, the settling time for the capacity transient as determined from the negative current response in Fig. 3*A* overlaps considerably with the rising phase of the asymmetry current).

A genuine rising phase of the asymmetry current, if it exists (Armstrong & Bezanilla, 1974; Nonner *et al.* 1978) will probably not be detected in the present study. Because of the time delay introduced by the settling of the clamp and the filters, a method of integration, rather than extrapolation, was used to calculate charge movement. Fig. 2 shows a drawing of a hypothetical 'on' gating current record to illustrate this method schematically. The time axis of the data

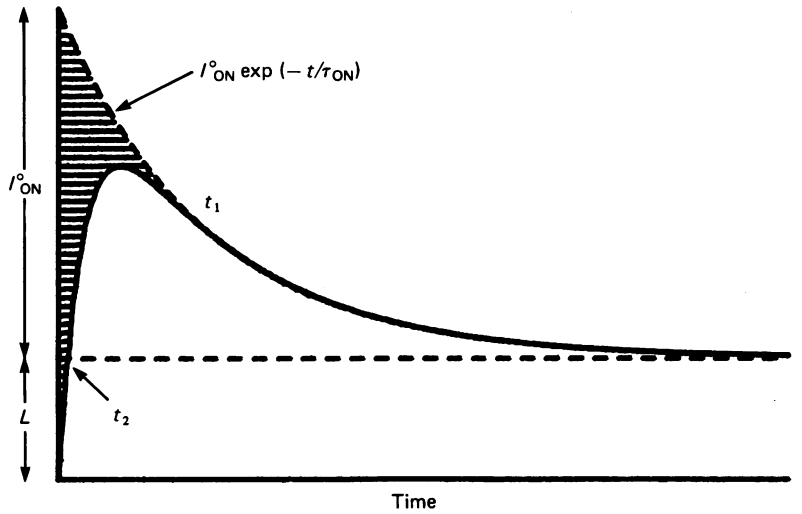

Fig. 2. Schematic drawing of asymmetry current. For analysis, t_1 was picked by eye and the expression $L+I^0_{on}\exp(-t/\tau^0_{on})$ fitted to the declining phase. L was introduced to account for a steady non-linear leakage or a slow component of asymmetry current.

points has been first shifted so that the origin coincided with the turning-on of the asymmetry current. From an arbitrary point in time t_1, the falling phase of the gating current was fitted to the expression

$$I_g = L+I^0_{on}\exp(-t/\tau_{on}), \tag{1}$$

with a programme similar to that used in fitting the Na current inactivation; L represents a steady asymmetry ionic leakage or a slow component for the asymmetry current. All charge movement in this paper was calculated as the area under the asymmetry current record after correcting for L. In the particular case when L is zero, the area under the gating current record was calculated as

$$Q = \int_{t_1}^{\infty} I^0_{on}\exp(-t/\tau_{on}) + \int_0^{t_1}(\text{data}).$$

The area under the current record for $0 < t < t_1$ was obtained by numerical integration. In the general case when L is non-zero we assume that the total asymmetry current is the sum of two terms:

$$I = I^0_{on}[\exp(-t/\tau_{on})-\exp(-t/\tau_a)]+L[1-\exp(-t/\tau_b)],$$

where the first term represents the asymmetry current component with a rising phase characterized by a time constant τ_a and the second term represents the non-linear ionic leakage current with a rising phase characterized by a time constant τ_b. If the non-linear ionic leakage current is not time-dependent, then τ_b will be determined by the finite settling time of the clamp and the filter characteristic of the low pass filters. For the gating current component, τ_a in general is expected to be larger than τ_b since τ_a not only includes contributions from the clamp settling time and the filters but also possibly, from a true rising phase of the asymmetry current. Ignoring this contribution from a true rising phase of the asymmetry current, all charge movements in

this paper are calculated with $\tau_a = \tau_b$. On this assumption, it can be shown that the asymmetry charge movement equals

$$Q = \int_0^\infty I_{on}^0 \exp(-t/\tau_{on}) - \left(\frac{I_{on}^0}{I_{on}^0 + L}\right) A_1, \quad (2)$$

where A_1 is the shaded area shown in Fig. 2.

Irrespective of the assumptions used for calculating charge movement, a lower limit on the

TABLE 1. Comparison of asymmetrical charge movement Q at +40 mV calculated in the different ways. Some of the parameters used in the calculations are also shown

Fibre	L (nA)	Q (fC)	Q_{lowest} (fC)	Q_{ext} (fC)	$\frac{Q-Q_{lowest}}{Q}$ (%)	τ_{on} (msec)	I^1 (nA)
1	0·05	52	51·3	64·9	1·3	0·044	1·48
2	0·21	91·2	82·5	113	9·5	0·039	2·89
3	0·12	42·1	41	50·4	2·6	0·039	1·29
4	0·96	51·3	46·5	51·2	9·3	0·013	3·94
5	0·003	50·9	50·9	56·6	0	0·041	1·38
6	0·05	113	111·6	138	1	0·052	2·66
7	0·048	85·6	84·9	88·7	1	0·034	2·61
8	0·44	38·7	36·6	39·5	5·4	0·03	1·32
9	0·18	29·3	28·6	39	2·4	0·026	1·5
10	0·16	69·5	67·5	72·4	2·9	0·036	2·0
11	0·17	43·0	40·8	56·3	5·1	0·027	2·1
			Mean ± S.E.				
	0·22 ± 0·08	61·0 ± 7·8	58·4 ± 7·6	70·0 ± 9·5	3·7 ± 1·0	0·035 ± 0·003	2·1 ± 0·25

L = determined by fitting eqn. (1) to the declining phase of the asymmetry current.

Q = calculated according to eqn. (2), as described in Methods.

Q_{lowest} = calculated according to the expression $\int_{t_1}^\infty I_{on}^0 \exp(-t/\tau_{on}) + \int_{t_2}^{t_1}$(data) (see Fig. 2).

Q_{ext} = calculated by extrapolating the declining phase of the asymmetry current back to onset of pulse (I^1) and then multiplying it with the fitted τ_{on}, after correcting for a filter delay of 10–30 μsec.

I^1 and τ_{on} = extrapolated current and time constant at 40 mV.

charge movement, Q_{lowest}, can be obtained by integrating the record starting at point t_2 (Fig. 2) after correcting for L according to the expression:

$$\int_{t_1}^\infty I_{on}^0 \exp(-t/\tau_{on}) + \int_{t_1}^{t_2} (\text{data}).$$

Table 1 shows a comparison of Q_{lowest} and Q calculated with eqn. (2) at 40 mV for all fibres in this paper. The largest difference between Q_{lowest} and Q is, as expected, found in fibres with a large non-linear leakage but the average fractional difference is very small; i.e. only 3·7%. Table 1 also shows the corresponding charge movement calculated by extrapolating the declining phase of the gating current to onset of the pulse (after correcting for filter delay introduced by the low pass filters). This extrapolated charge Q_{ext} is about 16% bigger than Q calculated according to eqn. (2).

Nodal capacity in the rabbit. Fig. 3 shows examples of the current response in a rabbit node associated with a negative pulse to −170 mV applied from −110 mV. From such records, a value for the nodal capacity (C_M) was obtained by calculating the charge carried by the transient capacity current in a manner similar to that used for calculating the asymmetry charge. The average value for C_M such determined for all fibres in Table 2 is 3·3 pF ± 0·8 (n = 11). This can be compared with the value of 3·9 pF in the frog node obtained in a similar way by Nonner *et al.* (1978).

Instrumental errors in charge measurement. Since asymmetry currents are an order of magnitude

smaller than normal ionic currents, it is important to evaluate errors in charge measurement arising from limited resolution and non-linearity of the recording system. First, the 12-bit analogue-to-digital converter has a fundamental resolution of 2·5 mV. Since current signals at the E-pool are typically amplified 20 times, a resolution of 0·12 mV at the E-pool is obtained which corresponds to 0·02 nA for an average R_{ED} value of 5·9 MΩ ± 0·9 (n = 11). This resolution in current signal is much smaller than the typical value for the peak asymmetry current of 1–2 nA at large depolarizations (for example, see Fig. 5). Secondly, the pulse generator has a maximal error of ± 0·1 mV in ± 100 mV. An error ΔE in the command voltage results in an error in charge measurement of $\Delta Q = C_M \Delta E$. The maximal test pulse used is about 150 mV; with C_M = 3·5 pF, this corresponds to a maximal error $\Delta Q \doteqdot 1.0$ fC.

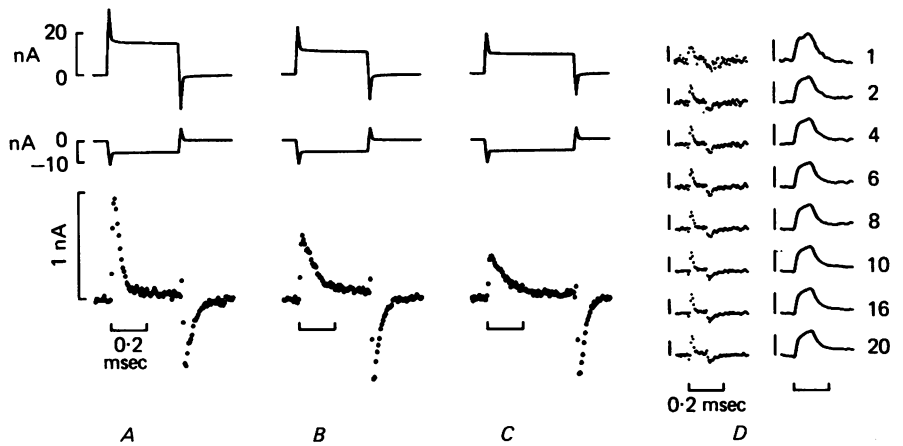

Fig. 3. Asymmetry current in a rabbit node of Ranvier at 17·9 °C. All external Na was replaced by 154 mM-TMA-Cl plus 300 nM-TTX. Both the positive and negative pulses were applied from a level of − 110 mV. The associated current responses were averaged (30 times positive, 90 times negative) and shown as the upper pair of records. The positive steps were to + 55 mV (*A*), + 10 (*B*) and − 5 mV (*C*) respectively. The negative steps were all to − 170 mV. From each pair of upper records, the asymmetry current (bottom) was calculated by first scaling the negative current response and then adding it to the positive current response. The scaling factor (i.e. size of positive pulse/size of negative pulse) was 2·75, 2, and 1·75 in *A*, *B* and *C* respectively. *D* shows how averaging more pulses reduces noise level of asymmetry current (left) and the associated integrated record (right). The number of positive responses averaged to obtain the record is shown beside each record. The vertical bars here indicate 2 nA (gating current) and 50 fC (integrated records). Current signal was low-pass filtered at 33 kHz and sampled at intervals of 7 μsec (*A*–*C*) and 5 μsec (*D*). The frequency of stimulation was 4 sec^{-1}. The ends of fibre were cut in 160 mM-CsCl. The temperature was 17·9 °C in (*A*) through (*C*) and 25 °C in (*D*).

RESULTS

Asymmetry currents in the rabbit node of Ranvier

Fig. 3 shows typical asymmetry current record at 17·9 °C associated with various test pulses to + 55 mV (*A*), + 10 mV (*B*) and − 5 mV (*C*). Sodium currents were eliminated by 300 nM-TTX and by replacement of external Na with TMA-Cl. Both the positive and negative pulses were applied from − 110 mV, and the averaged current responses were shown as a pair of continuous traces (upper). From each pair, the corresponding asymmetry current (bottom) was calculated by summing the

positive current response with a scaled negative response, the scaling factor in each case being (size of positive pulse/size of negative pulse).

A transient outward charge movement is associated with the onset of the test pulse which is followed by a reverse charge movement when the pulse terminates. The time constant for the 'on' charge movement (fitted with a single exponential, see Methods) decreased with increasing test potentials, from 0·09 msec at −5 mV

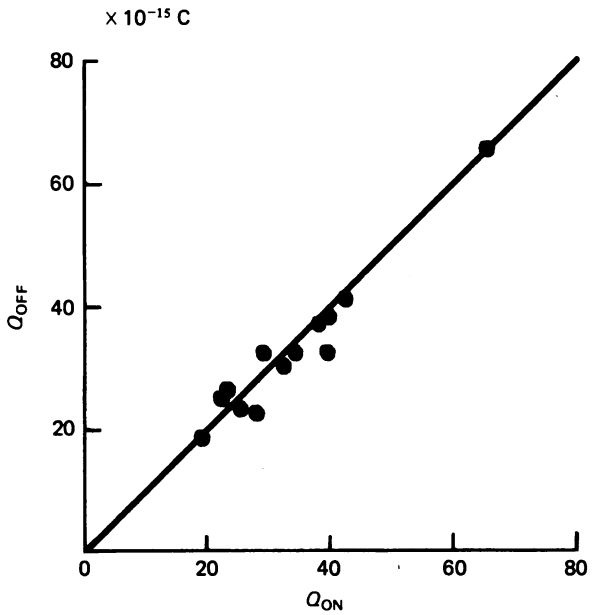

Fig. 4. Plot of Q_{on} *vs.* Q_{off}. Test depolarizations to between −57·5 and −5 mV with durations ranging 0·9–0·3 msec were used. The continuous line is drawn with a slope of one. Data are from five fibres. Both positive and negative pulses were applied from −(102·5–110) mV. Temperature 17·9–23·4 °C.

(*C*) to 0·03 msec at +55 mV (*A*), whereas the 'off' time constant remained roughly constant at around 0·038 msec. Fig. 3*D* shows the effect of averaging more pulses on the noise level of the asymmetry current. Here, the number of positive responses which were averaged in order to obtain the asymmetry current was increased progressively from one (top) to twenty (bottom). Clearly, signal averaging reduced the noise level; but it did not lead to any significant change in the shape of the individual asymmetry current record (left) or of the corresponding integrated record (right).

Intramembranous origin of the asymmetry current

To justify the conclusion that the asymmetry current reflects displacement of particles within the membrane it is necessary to show that the charge displaced during the onset of a test pulse is equal to, but opposite in sign to, the charge displaced during the offset of the test pulse; and, furthermore there should be a saturation of charge displacement (Armstrong & Bezanilla, 1974; Keynes & Rojas, 1974; Nonner *et al.* 1975). Experiments with the test pulses up to −5 mV show that

there is indeed equality of the 'on' and 'off' charge movement; for example in Fig. 3*C* the two values Q_{on} and Q_{off} calculated as described in the Methods were 42·4 and 41·1 fC respectively. Similarly, in Fig. 4, which summarizes results from five experiments, the 'on' charge movement is plotted against the 'off' charge movement associated with 0·9–0·3 msec test pulses to potentials between −57·5 and −5 mV. Clearly, the data points lie close to the line of equality (slope 45°) thus

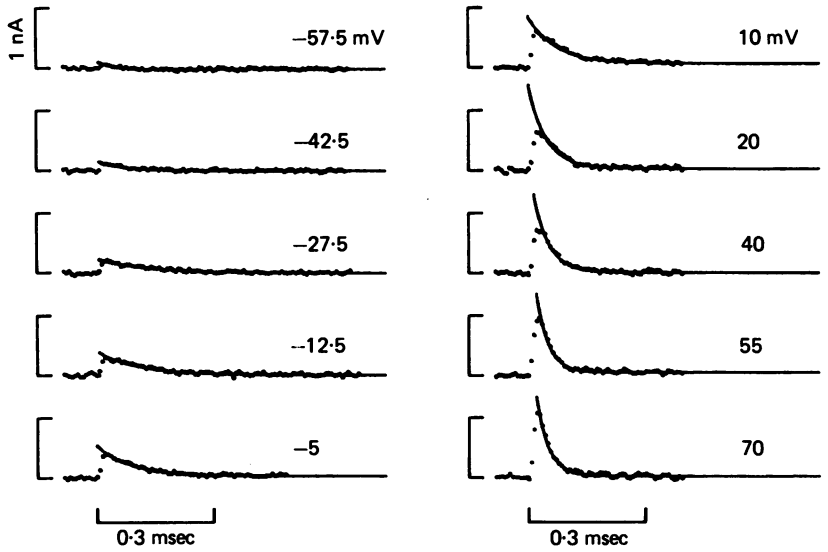

Fig. 5. Asymmetrical currents associated with pulses of increasing amplitude. Only the 'on' responses are shown. The initial membrane potential was −110 mV and test depolarizations were to the potentials indicated in each record. The continuous curve in each record is a least-squares fit to the declining phase of the asymmetrical current according to eqn. (1). L is around 0 nA at the smallest depolarization (to −57·5 mV) and is 0·003 nA at the largest depolarization (to +70 mV). Temperature, 17·9 °C.

satisfying the criterion of charge balance. A more complicated kind of charge balance is observed when larger test pulses are used, as will be described later in the section on charge immobilization. The second criterion, i.e. the existence of charge saturation, was also satisfied, as illustrated by the experiment shown in Fig. 5. The 'on' charge movement associated with a series of increasing test steps (−57·5 to 70 mV) is shown in Fig. 5. Clearly, as the test step became more positive the displaced charge reaches a saturating value (of about 50 fC) for test steps more positive than −5 mV (Fig. 5). The time constant (τ_{on}) for the declining phase of each gating current record was determined by fitting it to a single exponential (continuous curves in Fig. 5). The value of τ_{on} at −5 mV among different fibres ranged from 0·035 to 0·089 msec (23·4–15 °C) with an average value of 0·062 msec at 18·8 °C ± 1·0 (Table 2). This variation of τ_{on} among fibres could reflect either an effect of temperature or fibre differences; more experiments are needed to resolve this question. Fig. 6*A*, *B* shows a plot of the voltage dependence of τ_{on} and charge movement from the experiment in Fig. 5. Following Keynes & Rojas (1974) and Nonner *et al.* (1975), I fitted the expression

$$Q(E) = Q_{max} \cdot [1 + \exp\{z_1 \bar{e} (E_1 - E)/kT\}]^{-1} \quad (3)$$

to the voltage-dependence of the charge movement. This expression describes the Boltzman distribution of charges with effective valence z_1 between two discrete energy levels; e is the absolute value of the charge on an electron. Q_{max} represents the maximal charge displacement and E_1 is the midpoint potential for the charge

TABLE 2. Summary of various parameters for the asymmetry current and Na current in the rabbit node of Ranvier

Fibre	T (°C)	E_{Na} (mV)	I_{Na} (nA)	$\bar{g}_{Na}$ ($\times 10^{-7}$ S)	Q_{max} (fC)	z_1	E_1 (mV)	τ_{on} (msec)	N ($\times 10^3$)	γ (pS)
1	15	85	30·9	5·9	56	1·9	−37	0·072	70	8·4
2	16	35	27	14·8	105	1·8	−39·1	0·066	131	11·3
3	15·6	37	22·6	9·2	50	1·5	−21·0	0·048	62	14·7
4	22·7	70	57·5	10·2	65	1·7	−26·3	0·037	81	12·5
5	17·9	—	30·8	3·5	52	2·1	−29·4	0·089	65	5·4
6	17·9	60	51·7	11·9	111	—	—	0·084	139	8·6
7	17·9	—	—	—	91	1·9	−27·5	0·076	114	—
8	16·1	70	24·7	5·3	44	—	—	—	55	9·6
9	23·4	63	19·7	5·2	32	2·2	−48·8	0·035	40	13
10	23·4	87	25·8	6·2	71	—	—	—	89	6·9
11	20·2	45	14·6	4·2	44	1·8	−37·5	0·054	55	7·6
					Mean ± S.E.					
	18·8	61	30·5	7·6	66	1·86	−33	0·062	82	9·8
	± 1·0	± 6·4	± 4·3	± 1·2	± 8	± 0·08	± 3	± 0·007	± 10	± 0·9

E_{Na} = reversal potential for Na (mV).
I_{Na} = peak Na current at −5 mV (nA).
$\bar{g}_{Na}$ = maximal Na conductance ($\times 10^{-7}$ S), determined from the Na current at −5 mV.
Q_{max} = maximal charge movement (fC).
z_1 = equivalent valence for $Q(E)$ curve.
E_1 = mid-point potential for $Q(E)$ curve.
N = upper limit for number of channels/node ($\times 10^3$).
γ = lower limit for single Na channel conductance (pS).
The $\bar{g}_{Na}$ value for fibre 5 was determined with the average E_{Na} of 61 mV. For fibres 6, 8 and 10, there were not enough points over the potential range needed for determination of z_1 and E_1 but there were enough points at large depolarizations to fit a plateau for determining Q_{max}. For all fibres, the largest depolarizations used in measuring asymmetry current were > 50 mV.

distribution. The continuous curve in Fig. 6B was calculated with Q_{max} = 52 fC, z_1 = 2·1 and E_1 = −29·4 mV. The corresponding voltage dependence of the time constant for a first order transition can be approximated by

$$\tau = \frac{2\tau_{max}}{\exp[z_1 e(E - E_1)/2kT] + \exp[-z_1 e(E - E_1)/2kT]}, \quad (4)$$

where τ_{max} is the maximum time constant reached at $E = E_1$ (Keynes & Rojas, 1974). The solid line in Fig. 6A represents this function using values of z_1 and E_1 determined from the fit to the charge and τ_{max} arbitrarily chosen as 0·135 msec. Table 2 summarizes the values for the parameters Q_{max}, z_1 and E_1 used in fitting expression (3) to the voltage-dependence of charge distribution in different experiments. The average values for Q_{max}, z_1 and E_1 for rabbit nodes are 66 fC, 1·86 and

-33 mV respectively; and they are clearly of the same order of magnitude as the corresponding values of 140 fC, 1·7 and -37 mV respectively for the asymmetry currents in the frog node (Nonner *et al.* 1975).

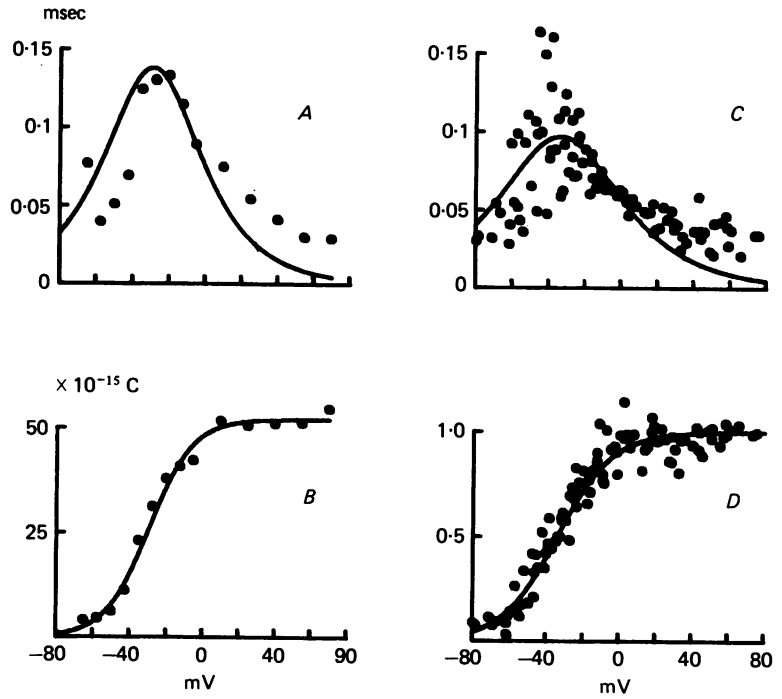

Fig. 6. The voltage dependence of the time constant τ_{on} (upper panels) and of the asymmetry charge movement Q_{on} (lower panels). *A* and *B* are from a single experiment (same fibre as in Fig. 5) and *C* and *D* are pooled data. The solid line in *B* was calculated from eqn. (3) with $E_1 = -29{\cdot}4$ mV, $z_1 = 2{\cdot}1$ and $\bar{Q}_{max} = 52$ fC. The continuous line in *A* was calculated from eqn. (4) with values for E_1 and z_1 taken from *B* and τ_{max} arbitrarily chosen to be 0·135 msec. The current signals were low pass filtered at a cut-off frequency of 33 kHz. The pooling of the results of eight such experiments (fibres 1–5, 7, 9, 11 in Table 2) are shown in *C* and *D*. This was achieved by first shifting both the Q_{on} and τ_{on} data files in each individual experiment along the voltage axis by $(-33-E_1)$ mV (see Table 2). Each shifted Q_{on} file is normalized with respect to its associated Q_{max} value. Each individual shifted τ_{on} file is first normalized with respect to its respective τ_{on} value extrapolated at -5 mV, then scaled by the corresponding average value at -5 mV from all experiments. The continuous line in *D* is a least-squares fit to the data obtained by first linearizing the data with respect to voltage (i.e. ln $(Q^{-1}-1)$), and then fitting a similarly linearized form of eqn. (3) to it over the range $0{\cdot}01 < Q < 0{\cdot}7$. The fitted value for z_1 is 1·71 (compare with the value for z_1 of 1·86 from Table 2). The continuous line in *C* is calculated as described above with τ_{max} arbitrarily chosen as 0·1 msec.

A way of plotting the results is shown in Fig. 6*C*, *D*. Both the $Q(E)$ and $\tau_{on}(E)$ data from each individual fibre were first shifted by $(-33-E_1)$ mV along the voltage axis so that the mid-point potential for all $Q(E)$ data matched, and then normalized as described in the legend of Fig. 6. Even though this way of pooling data is arbitrary,

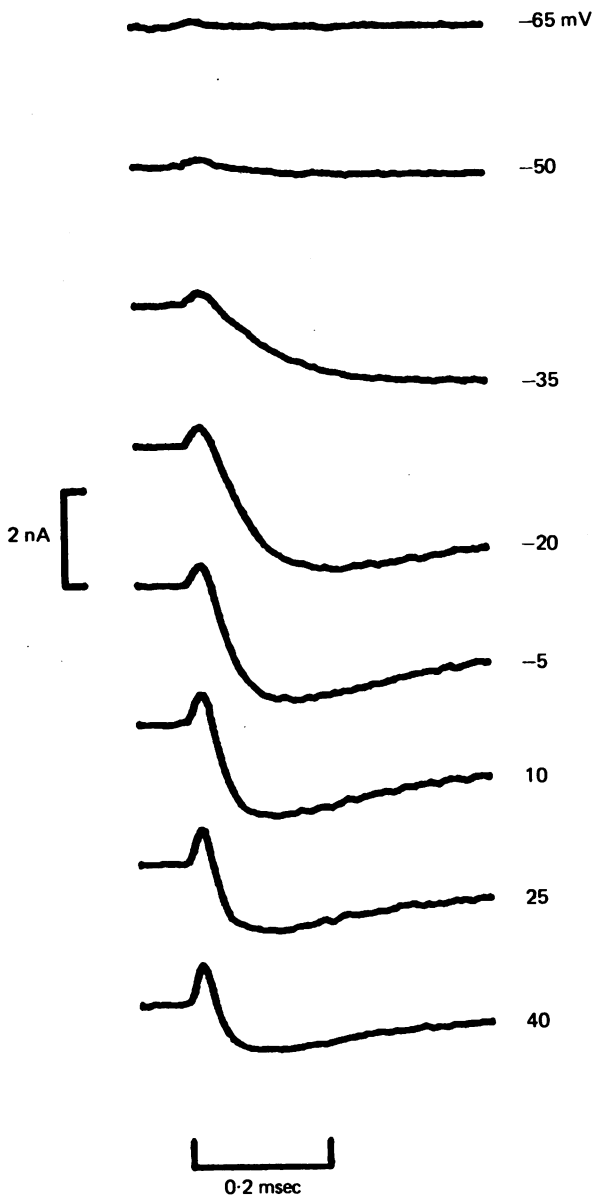

Fig. 7. Simultaneous recording of asymmetry and Na current in a rabbit node at 25 °C. The family of current records shown were obtained in 20 nM-TTX-Locke using a series of increasing test steps from −65 mV (top) to 40 mV (bottom) after subtraction of the linear leakage and capacitative current. Both the positive and negative steps were applied from −110 mV.

it nevertheless shows the similarity of shapes of the respective data curves from different experiments and in particular the consistent observation of charge saturation.

The relation of the asymmetry current to activation of the Na channel

A fundamental criterion that any 'gating' current must satisfy is that it begins to flow at least by the time the channel opens (Hille, 1975). This could be seen in

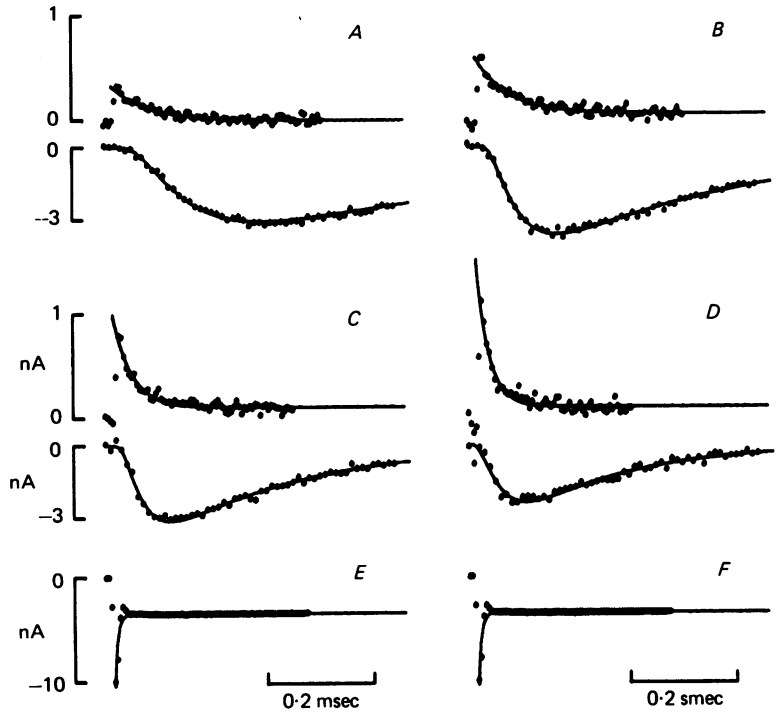

Fig. 8. Kinetic comparison between the asymmetry current and the activation of Na current in the same rabbit node at 25 °C. Each pair of traces is associated with a fixed test potential to *A*, −35 mV; *B*, −20 mV; *C*, −5 mV; and *D*, 10 mV. The upper record in each pair is the asymmetry current and the lower record is the sodium current (corrected for asymmetry current). The continuous curves in asymmetry current records are fits using eqn. (1). The continuous curves in Na current records represent fit to the expression

$$[1-\exp(t_D-t)/\tau_m]^2[C+A\exp(-t/\tau_h)], \text{ where } 1-\exp(t_D-t)/\tau_m=0 \text{ for } t<t_D.$$

The procedure for this fit involved first fitting the function $C+A\exp(-t/\tau_h)$ to the Na current inactivation using the programme described in Methods. Dividing the Na current by this function yielded a hypothetical non-inactivating current record, which was then fitted to the expression $\{1-\exp[(t_D-t)/\tau_m]\}^2$, with t_D chosen arbitrarily (0–0·03 msec). The fit for the Na current was then reconstructed from these two fits. The fitted values in msec for τ_{on} and τ_m are, respectively: 0·07 and 0·09 in *A*; 0·064 and 0·048 in *B*; 0·036 and 0·036 in *C*; and 0·024 and 0·04 in *D*. Records *E* and *F* show two identical leak current traces associated with a hyperpolarizing step to −155 mV. The solid line was fitted to the declining phase of the capacity current with eqn. (1) and has a time constant of 0·0056 msec, which can be compared with the smallest τ_m value of 0·036. Na currents were obtained from measurements in the presence of 20 nM-TTX, and were corrected for the associated asymmetry (using the fitted curves for the respective asymmetry current record). The test pulses for both asymmetry and Na current were applied from −110 mV. All current signals were filtered by a 4-pole Bessel filter (33 kHz) and sampled at intervals of 5 μsec (asymmetry current) and 10 μsec (Na current).

Fig. 7, which shows a family of simultaneous recording of asymmetry and Na current associated with a series of increasing depolarizations, obtained in 20 nM-TTX. Fig. 8 shows a quantitative kinetic comparison between asymmetry and Na current from a different node at 25 °C at four different test potentials: -35 mV (A), -20 mV (B), -5 mV (C) and 10 mV (D). In each panel, the top record is the asymmetry current and the middle record its associated Na current. Clearly, the peak

TABLE 3. Comparison of τ_m and τ_{on} at 24·1 °C

E (mV)	τ_m (msec)	τ_{on} (msec)
−50	0·147	0·054
−42·5	0·099	0·038 ± 0·025(2)
−35	0·18 ± 0·093(2)	0·058 ± 0·007(2)
−20	0·057 ± 0·017(2)	0·048 ± 0·017(2)
−5	0·043 ± 0·005(4)	0·03 ± 0·005(3)
10	0·028 ± 0·002(4)	0·021 ± 0·002(4)
25	0·021 ± 0·001(2)	0·014 ± 0·003(3)

E = test potential.

τ_m = fitted from Na currents in the presence of 10–20 nM-TTX uncorrected for asymmetry current (see text and legend of Fig. 7 for details of fit).

τ_{on} = fitted from the asymmetry current using eqn. (1).

Test pulses for Na current and asymmetry currents were applied from a level of −(102·5–110) and −110 mV respectively. The average value for τ_c (time constant for capacity transient, see Fig. 8E) in these experiments was 0·006 msec.

outward flow of the asymmetry current precedes, and its subsequent decline overlaps, the activation of the Na current. The continuous curves in these records represent fits to the asymmetry current and Na current using eqn. (1) and the function $\{1-\exp[(t_D-t)/\tau_m]\}^2$. $[C+A\exp(-t/\tau_h)]$ respectively (see legend of Fig. 8 for details). The values for τ_{on} and τ_m in Fig. 8 are similar, being respectively, 0·07 and 0·09 msec at −35 mV, 0·064 and 0·048 msec at −20 mV, 0·036 and 0·036 msec at −5 mV and 0·024 and 0·04 msec at 10 mV. Such comparisons were made in five different experiments at 24·1 °C ± 0·6, and the results are summarized in Table 3. A more meaningful kinetic comparison is to compare the time course of charge transfer (integral of asymmetry current) with that of activation of Na conductance, as shown in Fig. 9. The data points on the left represent the normalized time course of Na activation after correcting for Na inactivation at various potentials. The continuous curve through these points represents fit to the function

$$m^2 = [1-\exp\{(t_D-t)/\tau_m\}]^2.$$

The continuous curves to the left of the data points represent the integral of the asymmetry current. The function m^2 and the charge transfer curve at each potential are replotted on the right with the two interrupted curves representing the square and third power of the charge transfer curve. Two points are noted. First, charge transfer preceded activation of Na conductance. Secondly, raising the individual charge transfer curve to second or third power did not yield a curve that matched

the corresponding activation of Na conductance (Neumke, Nonner & Stämpfli, 1977).

Charge immobilization. Stronger evidence for relating the asymmetry current to gating of the Na channel in the rabbit comes from the observation that the gating charge movement was inactivated by large depolarizations, as has been reported

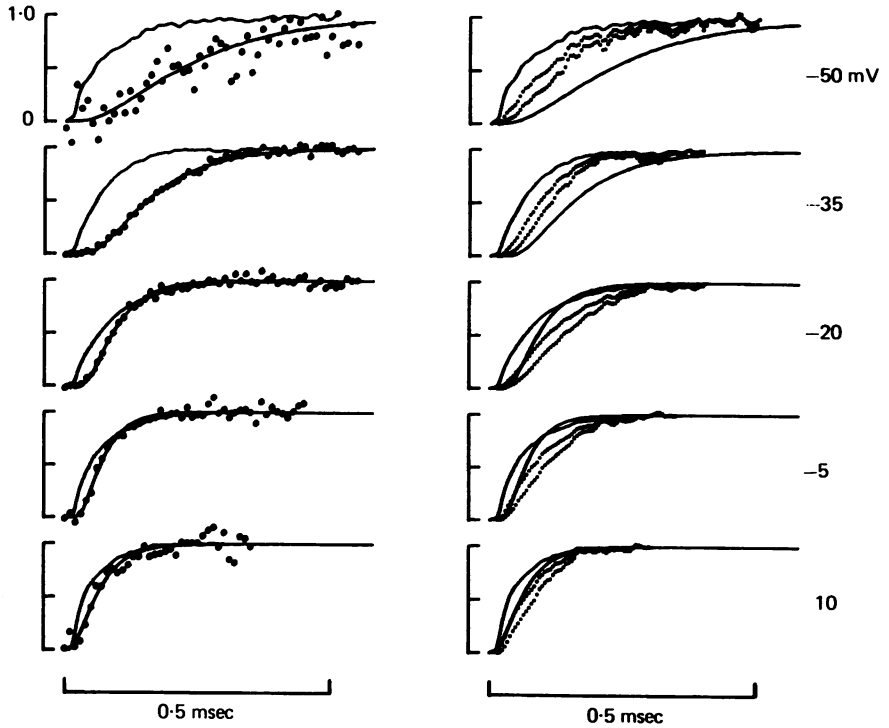

Fig. 9. Kinetic comparison between time course of charge displacement and activation of the Na conductance at 25 °C. Data from the same fibre as Fig. 8. In the left-hand records, the data points are the normalized values for Na activation after correcting for Na inactivation at each indicated potential, computed as $I_{Na}/[A \exp(-t/\tau_h)+C]$. The continuous curves through the data represent the fit to the function

$$m^2 = [1-\exp(t_D-t)/\tau_m]^2, \text{ with } m^2 = 0 \text{ for } t < t_D.$$

The continuous curves to the left of the data points are the normalized time courses of charge transfer, obtained by integrating the asymmetry current record after first subtracting a constant L from it; the curves have been normalized with respect to the integrated charge value at the end of the asymmetry current record. L is determined by fitting eqn. (1) to the last 0·2–0·3 msec portion of the asymmetry current record. The right-hand records show the function m^2 and the corresponding charge transfer curve replotted for each potential. The two interrupted curves at each potential are computed from the charge transfer curve by raising it to the second and third powers.

previously for frog and squid (Armstrong & Bezanilla, 1977; Nonner, Rojas & Stämpfli, 1978). This is best seen by integrating the asymmetry current with respect to time to yield the time course of charge transfer (Nonner, 1979). Fig. 10*A* shows such an integrated record associated with a small test pulse to −42 mV. The charge transfer during the test step shows a fast saturating component which returns

quickly when the pulse terminates. However, as Fig. 10*B* shows, when a much larger test step to 70 mV was used the quick return of charge at the end of the pulse accounted only for part of the charge displaced during the test pulse; the remainder apparently returned much more slowly. Furthermore, it is seen that most charge returns quickly when the pulse is short, but not (only about 30 %) when the pulse is long (0·6 msec).

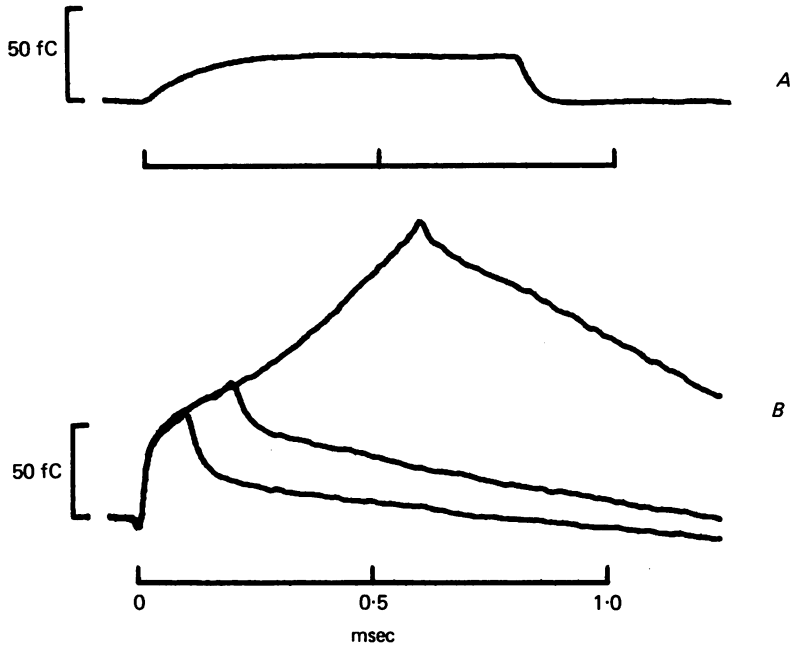

Fig. 10. Immobilization of asymmetry current in the rabbit node of Ranvier. The total asymmetry current was integrated with respect to time to yield the time course of charge transfer. The test pulse was to −27·5 mV in *A* and +70 mV in *B*. In *B*, the effect of changing the duration of the test pulse on the net charge transfer is shown by superimposition of results obtained with different pulse durations.

Note that in *B* but not in *A*, the charge returns in a fast phase (within 0·1 msec) and a slow phase. The fast return of charge accounts for all in *A*, but only part in *B*, of the charge initially displaced during the test pulse. Lengthening the test pulse duration diminishes the component of fast charge return but enhances the slow return (*B*). Quantitative analysis of the slow component is difficult since existence of a small non-linear ionic leakage would lead to a significant charge error when the currents are integrated (for example, integration of a non-linear ionic current of 0·2 nA (see Table 1) for 1 msec results in an error in charge of 200 fC). The test pulses were applied from a reference level between −102·5 and −110 mV. *A* and *B* are from different fibres. Temperature is 18 °C in *A* and 25 °C in *B*.

The above considerations, plus the observation that the steady-state properties of the rabbit asymmetry current are so similar to those of frog (see preceding section), lead us to assume that the asymmetry charge movements recorded in this paper in the rabbit nodal membrane are indeed 'gating' currents for the Na conductance, as has been suggested for the squid and frog nerve (Armstrong & Bezanilla, 1974; Keynes & Rojas, 1974; Rojas & Keynes, 1974). With this assumption, limiting values

for the number of Na channels and their single channel conductance in a rabbit node can now be estimated if the charge movement required to open each Na channel is known.

The minimum charge movement required to activate a single rabbit Na channel

Assuming that the Na channels are independent and have only two conductance states, the theoretical minimum charge required to activate one channel can be determined from the following equation with small p.

$$Q_{\min} = kT \frac{\mathrm{d}}{\mathrm{d}E}[\ln\{p/(1-p)\}], \tag{5}$$

where p is the probability of a channel being open (Hodgkin & Huxley, 1952; Almers, 1978; Sigworth, 1980). p is experimentally determined as the ratio of the peak sodium current (I_p) to the instantaneous current (I_s) measured at the same potential, and normalized to unity at large depolarizations as described by Neumcke *et al.* (1977) and Sigworth (1980). This method of evaluating p avoids the ambiguities in different choices for the theoretical current–voltage relations of the open channels. Series resistance error was minimized by reducing current size with TTX, and by electronic compensation of the series resistance. Fig. 11 shows such an experiment at 25 °C done with 20 nM-TTX and a series resistance compensation of 0·7 MΩ. Fig. 11*A* shows the $I_p - E$ and $I_s - E$ relation measured at the same potentials. *B* shows $p(E)$, determined as $p = I_p/I_s$, normalized to unity at +32·5 mV, and *C* shows $\ln[p/(1-p)]$ *vs.* voltage. It can be seen that the slope of $\ln[p/(1-p)]$ stays almost constant at 0·22 mV^{-1} (straight line in *C*) as p varies by more than two orders of magnitude from 0·004 to 0·5 over the potential range −71 to −42·5 mV. The right of Fig. 11 shows a series of sodium currents from the same experiment illustrating the steep, but graded, voltage dependence of the peak current over this potential range. The average value of the slope for four fibres, obtained in similar fashion, was 0·2 mV^{-1}, which corresponded to a minimum charge movement $Q_{\min} = 5{\cdot}0 \pm 0{\cdot}3$ electronic charges per channel at $22{\cdot}7 \pm 2$ °C. This value is very similar to the value of 6 in the squid (Hodgkin & Huxley, 1952) and 5 in the frog (Sigworth, 1979).

Bounds for N and γ in rabbit node

The major findings of this paper are summarized in Table 2. For each fibre, the measurements necessary for the determination of $\bar{g}_{Na}$ were done at the beginning of each experiment. Na-free solutions containing TTX were immediately applied and Q_{max} determined. On the assumption that the minimum gating charge to open each channel is $5\bar{e}$ for all experiments, the number of channels per node N was calculated as $N = Q_{max}/5\bar{e}$ and the single channel conductance γ is calculated as $\gamma = 5\bar{e}(\bar{g}_{Na}/Q_{max})$ (since $\bar{G}_{Na} = N\gamma$). Two points should be emphasized here. The first is that the present method of determining γ is freed from errors in calibration of nodal currents arising from uncertainties in measurement of the internodal resistance (R_{ED}). The reason is that γ is determined from the ratio of two terms, $\bar{g}_{Na}$ and Q_{max}, both of which are calculated using the same R_{ED} value in each individual fibre. The second point is that the calculations yield, respectively upper and lower limits for the

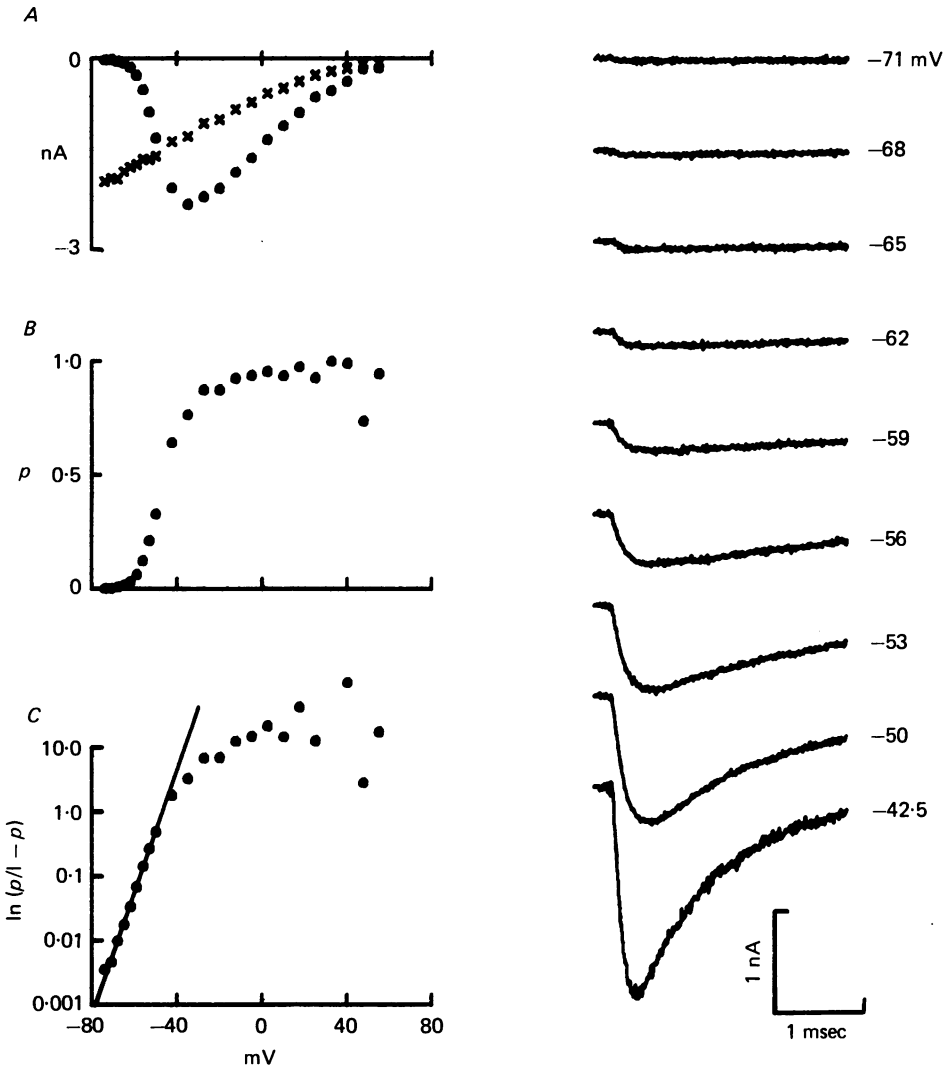

Fig. 11. Ratio of open and unopen channels at the time of peak sodium current at 25 °C. The fraction of channels open (p) was estimated from the ratio of peak current and the current of the same depolarization in the instantaneous I–E relation, and was normalized to unity at E = 32·5 mV. No prepulse was used. *A*, peak I–E relation (●) and instantaneous I–E relation (×) determined at the same depolarizations. *B*, plot of p *vs.* voltage. p = peak current/instantaneous current and is normalized to unity at + 32·5 mV. *C*, plot of ln $p/(1-p)$ *vs.* voltage. The continuous line has a slope of 0·22 mV^{-1}. Each data point corresponds to an average of four to sixteen current responses. The instantaneous current was determined by fitting a single exponential to the initial 0·06–0·1 msec of the tail current after a 0·2 msec activating pulse to 55 mV, and extrapolating to the end of the activating pulse after correcting for a filter delay of 14 μsec (33 kHz). A series resistance compensation of 0·7 MΩ was used and about 20 nM-TTX was used to decrease Na current by 70 %. The right-hand records show a series of Na current from the same experiment over the potential range −71 to −42·5 mV as indicated.

values of N and γ (since the identification of all asymmetry charge movement as related to Na channel gating need not be valid (Kimura & Meves, 1979) and since $5\bar{e}$ is only the minimum charge movement per channel). From Table 2, N ranges 40,000–139,000 per node and γ ranges 5·4–14.7 pS at 15–23·4 °C. The average value for γ in rabbit nodes of $9{\cdot}8 \pm 0{\cdot}9$ pS at $18{\cdot}8 \pm 1{\cdot}0$ °C is slightly higher than the value of 6–8 pS for frog nodes determined from noise experiments (Conti, Hille, Neumcke, Nonner & Stämpfli, 1977; Sigworth, 1977), probably because (*a*) their experiments were done in a lower temperature range of 4–13 °C. However, using a Q_{10} value of 1·72 for the Na conductance determined for the rabbit node over the temperature range 6–25 °C (Chiu, Mrose & Ritchie, 1979*a*), the present γ value of 9·8 pS at 18·8 °C would be scaled down to around 5·6 pS at 8 °C; also (*b*) the Locke solutions used for rabbit nodes have higher Na concentrations; (*c*) different methods were used to estimate γ; and, (*d*) rabbit and frog nodes have inherently different γ values. In spite of these differences, it must be concluded that γ in rabbit is very similar to frog. The average number of channels per rabbit node is 82×10^3 and this is similar to the two recent estimates of N in the frog node of 10^5 (Conti *et al.* 1976) and 10^4 (Sigworth, 1977) by noise analysis.

DISCUSSION

The major finding of this paper is that asymmetry currents occur in rabbit nodal membrane that are quite similar to the gating currents recorded in frog and squid nerve. On this basis, it is estimated that there are at most 82,000 Na channels in a rabbit node of Ranvier each having a conductance of at least 9·8 pS at 18·8 °C. These values, again, are similar to the corresponding values of 10^4–10^5 and of 6–8 pS, respectively, found in the frog node (Conti *et al.* 1976; Sigworth, 1979); and they support the conclusion of previous experiments that the maximal Na conductance is about the same in these two nerves (Chiu *et al.* 1979*a*). However, this latter conclusion is still in apparent conflict with the binding data of Ritchie (1978; see also Ritchie & Rogart, 1977) that the binding capacity for TTX is five times higher in the rabbit than in the frog, implying there are 5 times more Na channels in the rabbit node.

One possible resolution to this paradox is that in a normal rabbit node of Ranvier some Na channels are distributed underneath the paranodal region around the node. These channels would contribute negligible currents under voltage-clamp conditions since they are shunted from the external nodal fluid by a large series resistance due presumably to constriction of the paranodal region. This suggestion is similar to a recent hypothesis by Brismar (1979) that K currents in a normal rat node are low because the K channels are located underneath the myelin in the paranodal region. In certain pathological conditions in which partial demyelination occurs these channels are exposed, leading to large observable K currents (Brismar, 1979).

It is clear from the data in this paper that a certain co-operativity among 'gating' particles is involved in the opening of one single mammalian Na channel. For example, the steady state $Q(E)$ curve can be described by movement of particles with an equivalent valence of about 2 (Table 2) whereas the steepest part of the activation curve for Na conductance implies $5\bar{e}$ are needed to open one channel, i.e. movement of two or three particles is required. Furthermore, the initial time course

for charge transfer lags behind, and is not as sigmoidal as the time course of activation of Na conductance (Fig. 9). A physical interpretation of the Hodgkin–Huxley equations implies that for squid nerve displacement of three 'm' particles is needed to activate one channel. In the present analysis with rabbit nodes, this model does not predict the observed time course for activation of sodium conductance by raising the fraction of charge displaced at any time to either the second or third power. This analysis is similar to that used by Neumcke *et al.* (1977) in frog, and confirms their finding. However, before any gating model can be tested critically, it is crucial to know how much of the observable charge movement (in Fig. 9) is indeed related to activation of the Na conductance. Unfortunately, there is at present no reliable criterion for determining how much, if any, of the asymmetry current is not related to sodium channel gating. In this respect, the asymmetry current recorded in a mammalian nerve is possibly more 'pure' than that recorded in frog and squid, since in most mammalian fibres the K current is low or virtually absent (Horackova *et al.* 1968; Chiu *et al.* 1979*b*; Brismar, 1979) and thus would not contaminate the Na asymmetry current with its associated asymmetry current. This may partially account for the fact that the maximal charge movement measured in this paper is somewhat smaller than that in frog (Nonner *et al.* 1975).

I thank Dr Fred Sigworth for helpful discussions and for suggesting the method for calculating the asymmetry charge. I would also like to thank Professor J. M. Ritchie for his help, and for providing the facilities for this work which was supported by a grant NS 12327 from the U.S. P.H.S. and by a grant RG 1162 from the United States National Multiple Sclerosis Society.

REFERENCES

ADAMS, D. J. & GAGE, P. W. (1976). Gating currents associated with sodium and calcium current in an Aplysia neuron. *Science, N.Y.* **192**, 783–784.

ALMERS, W. (1978). Gating currents and charge movements in excitable membranes. *Rev. Physiol. Biochem. Pharmacol.* **82**, 96–190.

ARMSTRONG, C. M. & BEZANILLA, F. (1973). Currents related to movement of the gating particles of the sodium channels. *Nature, Lond.* **242**, 459–461.

ARMSTRONG, C. M. & BEZANILLA, F. (1974). Charge movement associated with the opening and closing of the activation gates of the Na channels. *J. gen. Physiol.* **63**, 533–552.

ARMSTRONG, C. M. & BEZANILLA, F. (1977). Inactivation of the sodium channel. I. Sodium current experiments. *J. gen Physiol.* **70**, 549–566.

BRISMAR, T. (1979). Potential clamp experiments on myelinated nerve fibres from alloxan diabetic rats. *Acta. physiol. scand.* **105**, 384–386.

BRISMAR, T. (1980). Potential clamp analysis of membrane currents in rat myelinated nerve fibres. *J. Physiol.* (in the Press).

CAHALAN, M. D. & ALMERS, W. (1979). Block of sodium conductance and gating current in squid giant axons poisoned with quaternary strychnine. *Biophys. J.* **27**, 57–73.

CHIU, S. Y., MROSE, H. E. & RITCHIE, J. M. (1979*a*). Anomalous temperature dependence of sodium conductance in rabbit nerve compared with frog nerve. *Nature, Lond.* **279**, 327–328.

CHIU, S. Y. & RITCHIE, J. M. (1980). Potassium channels in the nodal and internodal axonal membrane of mammalian myelinated fibres. *Nature, Lond.* (in the Press).

CHIU, S. Y., RITCHIE, J. M., ROGART, R. B. & STAGG, D. (1979*b*). A quantitative description of membrane currents in rabbit myelinated nerve. *J. Physiol.* **292**, 149–166.

CONTI, F., HILLE, B., NEUMCKE, B., NONNER, W. & STAMPFLI, R. (1976). Measurement of the conductance of the sodium channels from current fluctuations at the node of Ranvier. *J. Physiol.* **262**, 699–727.

HILLE, B. (1976). Gating in sodium channels in nerve. *A. Rev. Physiol.* **38**, 139–152.

HODGKIN, A. L. & HUXLEY, A. F. (1952). A quantitative description of membrane current and its application to conduction and excitation in nerve. *J. Physiol.* **117**, 500–544.

HORACKOVA, M., NONNER, W. & STAMPFLI, R. (1968). Action potentials and voltage-clamp currents of single rat Ranvier nodes. *Proc. int. Union physiol. Sci.* **7**, 198.

KEYNES, R. D. & ROJAS, E. (1974). Kinetics and steady-state properties of the charged system controlling sodium conductance in the squid giant axon. *J. Physiol.* **239**, 393–434.

KIMURA, J. E. & MEVES, H. (1979). The effect of temperature on the asymmetrical charge movement in squid giant axons. *J. Physiol.* **289**, 479–500.

KOSTYUK, P. G., KRISHTAL, O. A. & PIDOPLICHKO, V. I. (1977). Asymmetrical displacement currents in nerve cell membrane and effect of internal fluoride. *Nature, Lond.* **267**, 70–72.

MEVES, H. (1974). The effect of holding potential on the asymmetry currents in squid giant axons. *J. Physiol.* **243**, 847–867.

NEUMCKE, B., NONNER, W. & STAMPFLI, R. (1977). Asymmetrical displacement current and its relation with the activation of sodium current in the membrane of frog myelinated nerve. *Pflügers Arch.* **363**, 193–203.

NONNER, W. (1979). Relations between the inactivation of sodium channels and the immobilization of gating charge in frog myelinated nerve. *J. Physiol.* **299**, 573–603.

NONNER, W., ROJAS, E. & STAMPFLI, R. (1975). Displacement currents in the node of Ranvier. Voltage and time dependence. *Pflügers Arch.* **354**, 1–18.

NONNER, W., ROJAS, E. & STAMPFLI, R. (1978). Asymmetrical displacement current in the membrane of frog myelinated nerve: early time course and effects of membrane potential. *Pflügers Arch.* **375**, 75–85.

RITCHIE, J. M. (1978). Sodium channel as a drug receptor. In *Cell Membrane Receptors for Drugs and Hormones – A Multidisciplinary Approach*, ed. Straub, R. W. & Bolis, L., pp. 227–242. New York: Raven.

RITCHIE, J. M. & ROGART, R. B. (1977). The density of sodium channels in mammalian myelinated nerve fibres and the nature of the axonal membrane under the myelin sheath. *Proc. natn. Acad. Sci. U.S.A.* **74**, 211–215.

SIGWORTH, F. J. (1977). Sodium channels in nerve apparently have two conductance states. *Nature, Lond.* **270**, 265–267.

SIGWORTH, F. J. (1980). The variance of sodium current fluctuations at the node of Ranvier. *J. Physiol.* **307**, 97–129.